



Dynamic Analysis of MICP-Stabilized Soil and Liquefiable Soil With Varying Salinity Levels

Nur A. Diana ¹, Ria A. Aryani Soemitro ^{1*}, Januarti J. Ekaputri ¹,
Trihanyndio R. Satrya ¹, Dwa D. Warnana ²

¹Department of Civil Engineering, Sepuluh Nopember Institute of Technology, Surabaya, Indonesia.

²Department of Geophysical Engineering, Sepuluh Nopember Institute of Technology, Surabaya, Indonesia.

Received 13 December 2024; Revised 11 March 2025; Accepted 21 March 2025; Published 01 April 2025

Abstract

This study investigates the liquefaction potential of soils at Yogyakarta International Airport (YIA), a high-risk seismic zone, and evaluates the efficiency of carbonate precipitation driven by microbial activity (MICP) stabilization under varying salinity situations. The purposes include understanding the dynamic response of natural and MICP-treated soils to seismic loads and assessing the role of salinity in soil behavior. Triaxial cyclic testing was conducted on remolded soil samples at a very loose density ($D_r = 10\%$) to simulate field situations, using *Bacillus Safensis*. Microbes and a biocementing procedure enhanced with 35% fly ash. Salinity levels of 0%, 1%, 2%, and 3.4% were tested by curing for 28 days. The outcomes reveal that untreated soils liquefied inside of 4–6 cycles at $r_u = 0.8$ for 0%, 2%, and 3.4% salinity. In contrast, 1% salinity delayed liquefaction to 14 cycles, thereby enhancing soil resistance. MICP-treated soils showed enhanced stiffness, decreased compressive strain, and extended resistance to liquefaction under dynamic loads. SEM and XRD analyses verified CaCO_3 deposition, particle bonding, and decreased pore space. The novelty lies in demonstrating the significant role of salinity in enhancing the MICP procedure and improving soil stability, providing a sustainable solution for mitigating liquefaction risks in saline coastal regions.

Keywords: Biocementing; Dynamic Soil; Liquefaction; MICP; Saline Soil.

1. Introduction

The phenomenon of soil liquefaction has attracted considerable attention because of its catastrophic outcomes in geologically unstable areas. An example of this is the dissolution of freshwater carbonates in the vicinity of the Collar Coalfield, which resulted in the loss of numerous lives and substantial damage to infrastructure [1, 2]. Despite extensive research on soil liquefaction, gaps persist in understanding the interplay among stratification, soil composition, and liquefaction susceptibility. This research seeks to fill these gaps by conducting a detailed investigation into the dynamic behaviors of stratified soil systems under cyclic loading situations. Previous studies on soil liquefaction have predominantly focused on homogeneous soil systems or those with specific fine content proportions, often oversimplifying the complexities of real-world stratified soil deposits. For example, early research emphasized liquefaction potential in homogeneous sandy soils, neglecting the significant role of stratification in influencing pore pressure dissipation and failure mechanisms [1–3]. However, case studies near tailing dams, alluvial plains, and marine deposits have highlighted the necessity of understanding the effects of stratified soil systems on liquefaction phenomena [1, 4–7]. Stratification, especially silt interlayers inside of sandy deposits, has been recognized as a crucial factor contributing to lateral spreading, sand boiling, and settlements during seismic events [8–11].

* Corresponding author: ria@ce.its.ac.id

<http://dx.doi.org/10.28991/CEJ-2025-011-04-010>



© 2025 by the authors. Licensee C.E.J, Tehran, Iran. This article is an open access article distributed under the terms and conditions of the Creative Commons Attribution (CC-BY) license (<http://creativecommons.org/licenses/by/4.0/>).

Experimental investigations using centrifuge modeling and cyclic triaxial tests have advanced our understanding of the role of stratification in liquefaction failures. For instance, centrifuge experiments have demonstrated how reduced permeability in silt layers affects pore pressure dissipation, triggering lateral spreading and settlement [6–9]. Similarly, studies on reclaimed grounds with underlying clay layers have provided insights into the mechanisms of void redistribution and strain localization under cyclic loading [1, 10–12]. Despite these advancements, the impact of variable silt seam thickness and the interaction among silt and sandy layers on liquefaction susceptibility remains inadequately explored. More recent studies have attempted to bridge this gap by examining stratified soil systems under dynamic situations. For instance, shaking table and centrifuge tests have elucidated the effects of silt-sand interlayers on excess pore pressure development and shear deformations [11, 13–16]. Numerical modeling and cyclic triaxial tests have further highlighted the influence of soil stratification on liquefaction resistance, particularly in coastal and marine environments due to salinity variations [17–22]. However, these studies often focus on specific scenarios, leaving broader questions regarding the dynamic behaviors of stratified soils under varying geological and environmental situations unanswered.

A promising development in this field is the utilization of Microbially Induced Calcite Precipitation (MICP) for soil stabilization. The MICP procedure, which leverages microbial metabolic activities to produce calcium carbonate deposits, has shown potential in enhancing soil strength and reducing liquefaction susceptibility [16, 23–25]. Yet, the influence of salinity fluctuations on MICP-treated soils remains insufficiently addressed, particularly for coastal regions susceptible to seawater intrusion. This study builds on the existing body of work by conducting a comprehensive series of cyclic triaxial tests and micro-characterization analyses on stratified soil specimens. The purposes are to:

- Investigate the impact of silt seam thickness and stratification on pore pressure evolution and axial deformation occurring during liquefaction.
- Perform the role of MICP in stabilizing liquefaction-prone soils under varying salinity conditions.
- Evaluate the shear modulus and stiffness characteristics of stabilized and unstabilized soil specimens.

This study significantly extends the existing body of knowledge by integrating Microbially Induced Calcite Precipitation (MICP) stabilization under varying salinity situations to address liquefaction risk, particularly in coastal regions. Unlike previous studies that mainly conducted MICP in static soil conditions, this research explores its application under cyclic loading conditions representative of seismic activity. These findings indicate that salinity significantly enhances the biocementation process, leading to improved soil strength and resistance to cyclic deformation. Previous works, such as Zhu et al. [9], Dejong et al. [26], and Yang et al. [27], have noted the interaction among salinity and microbial activity but did not consider cyclic loading in seismic scenarios. This study thus bridges an important research gap and provides novel insights into the interplay among salinity, MICP, and dynamic soil behavior.

2. Materials and Experimental Setup

2.1. Research Area

The research location is administratively situated in Palihan, Kulonprogo Regency, Special Region of Yogyakarta, Indonesia, at coordinates (7°53'48.4" S - 110°3'18.9" E). The runway at YIA is located at an elevation of four meters above sea level, approximately 400 meters from the shoreline, as shown in Figure 1.



Figure 1. Location of the Study Area

Figure 1 depicts a map of the country published by the Ministry of Energy and Mineral Resources and the Geological Agency, which indicates the relative risk of liquefaction in various zones. The map reveals that YIA airport is situated in a zone marked in purple, indicating a high risk of liquefaction. This information provides the rationale for selecting this airport as a research site, given its status as a key piece of infrastructure in the Yogyakarta area.

The lithology of the area surrounding the YIA airport is characterized by the presence of fine sand-sized sedimentary rock with good sorting. This sand displays a loose and uncompacted situation, even in instances where the sedimentation has undergone weathering. The soil is composed of iron minerals and lithic andesite. The sedimentary procedure is fluvio-marine, as the research location is situated downstream by the river, resulting in a lower erosion rate than the sediment. In the south, these sediments undergo leaching by high sea waves along the coastline, resulting in a relatively uniform grain size. These sediments cover almost the entire area within the airport vicinity. At a depth exceeding 4.6 meters, the lithology comprises sandstone that has been cemented and transported by the Bogowonto to the west and Serang River to the east. This is due to the presence of sediments by adhesion properties that are well cemented, along with the compression procedure resulting from the loading of younger sediments above it, as can be seen in Figure 2 [22].

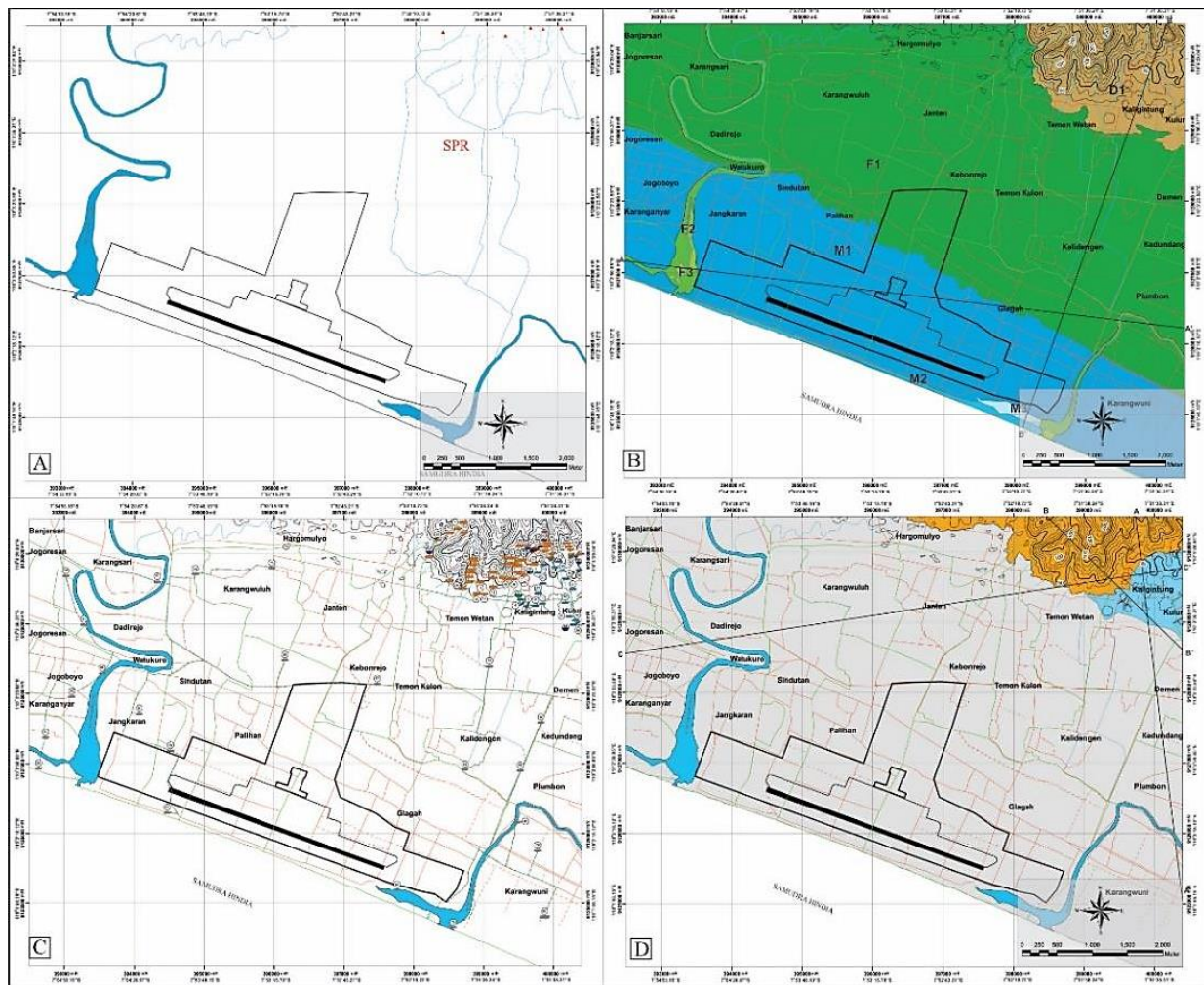


Figure 2. Map of the study area (a) drainage pattern, (b) geomorphology, (c) trajectories and observation locations, and (d) geology

2.2. Materials

In this study, sandy soil from the research site was used, with a gradation of sand grain sizes ranging from 0.005 mm to 2 mm. The soil was then mixed with fly ash type C at a percentage of 35%. This percentage was chosen based on previous research, which indicated that it produced optimal results for the variation in fly ash addition. The introduction of bacteria into this biocementing procedure utilized *Bacillus Safensis*. Bacteria were added with 0.2 ml of bacterial liquid in each triaxial cyclic sample. This was conducted to ascertain the durability of the biocementing procedure when subjected to dynamic loads, particularly in coastal situations. NaCl was added to model salinity variations at specified percentages of 0%, 1%, 2%, and 3.4% [28]. The initial soil density is modeled according to the relative density field, as determined by the following formula:

$$Dr = \frac{e_{max} - e}{e_{max} - e_{min}} \tag{1}$$

The initial soil density value can be obtained by the aforementioned formula, which can then be used to model the density of the remolded sample for the triaxial cyclic test.

$$\gamma_d \text{ models} = \frac{Gs \times \gamma_w}{1 + e} \tag{2}$$

Particle shape characteristics have been systematically analyzed for a randomly selected set of soil grains, as detailed in the following section.

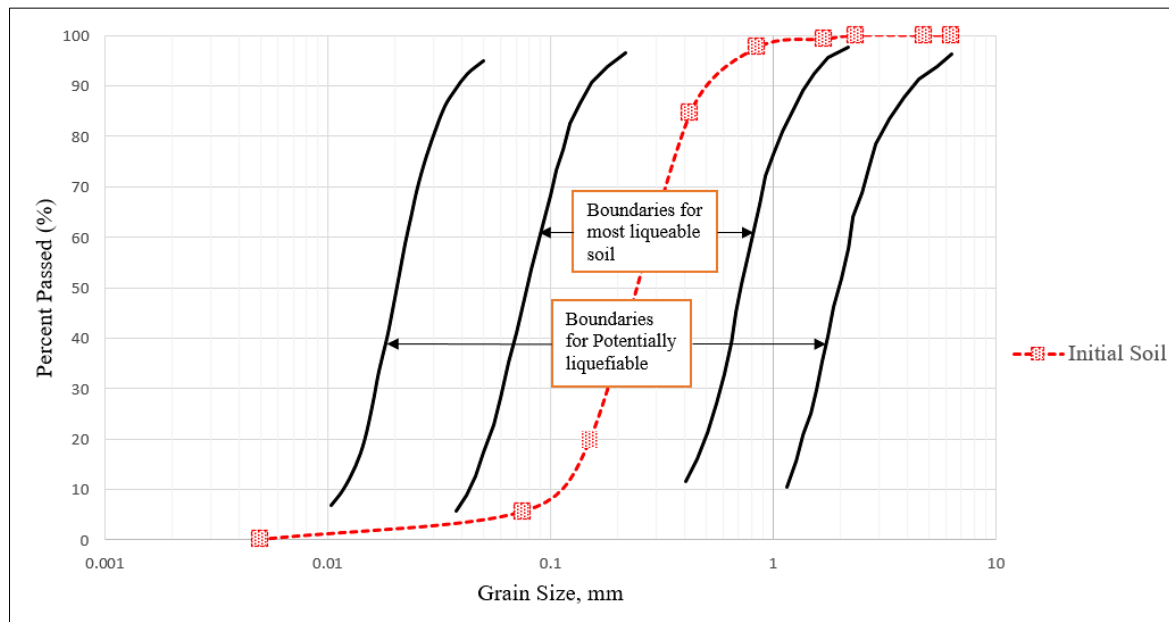


Figure 3. Grain distribution graph (Tsuchida (1970) [29])

The liquefaction-prone grain distribution graph by Miyamoto et al. (1988) [30] indicates that the initial soil situation is situated inside of the zone of highest liquefaction potential [17]. This is evidenced by Figure 3, which also exhibits the following physical properties (Table 1):

Table 1. Soil property index

Soil Parameters	Unit	
Water Content (w)	%	26.47
Specific Gravity (Gs)		3.12
Density (γt)	g/cm ³	1.60
Dry Density (γd)	g/cm ³	1.20
Cohesion (c)	kg/cm ²	1×10 ⁻¹⁶
Friction Angel (ø)	°	21.81
Sieve Analysis	%	96.86 (Sand)

Based on the soil data mentioned above, the relative density value is less than 1, indicating that when $Dr < 15$, it is classified as very loose sand. The samples have been adjusted to reflect field conditions with a relative density (Dr) of 10%, mirroring the characteristics of very loose sand soil.

The purpose of this study is to assess the potential of using fly ash as a cementation material and a calcium source in the biocementation process. This approach is particularly relevant given the abundance of fly ash waste generated by the combustion of new coal in steam power plants in Indonesia. In this study, we employed fly ash type C from Pacitan, Indonesia, with a detailed chemical composition determined by XRF testing conducted by YIA Soil and fly ash, as outlined in Table 2 [18].

Table 2. XRF test result

Oxides	Units	YIA Soil	Fly Ash
SiO ₂	%	47.86	20.28
Al ₂ O ₃	%	19.77	8.36
Fe ₂ O ₃	%	12.20	27.14
CaO	%	6.75	26.44

Salinity variations were tested by adding salinity levels of 0%, 1%, 2%, and 3.4% using NaCl as the salt content material in grams. Microbial fluid selection has been conducted in previous studies using *Bacillus Safensis*. bacteria that can survive in extreme and highly saline environments. These microbes produce urease and protease enzymes that are beneficial for the biocementing procedure to produce CaCO₃, which reacts with the addition of fly ash (Ca²⁺) and enzymes produced by the microbes. This reaction results in the cementing that binds the grains among particles, as shown in Figure 4 [12].

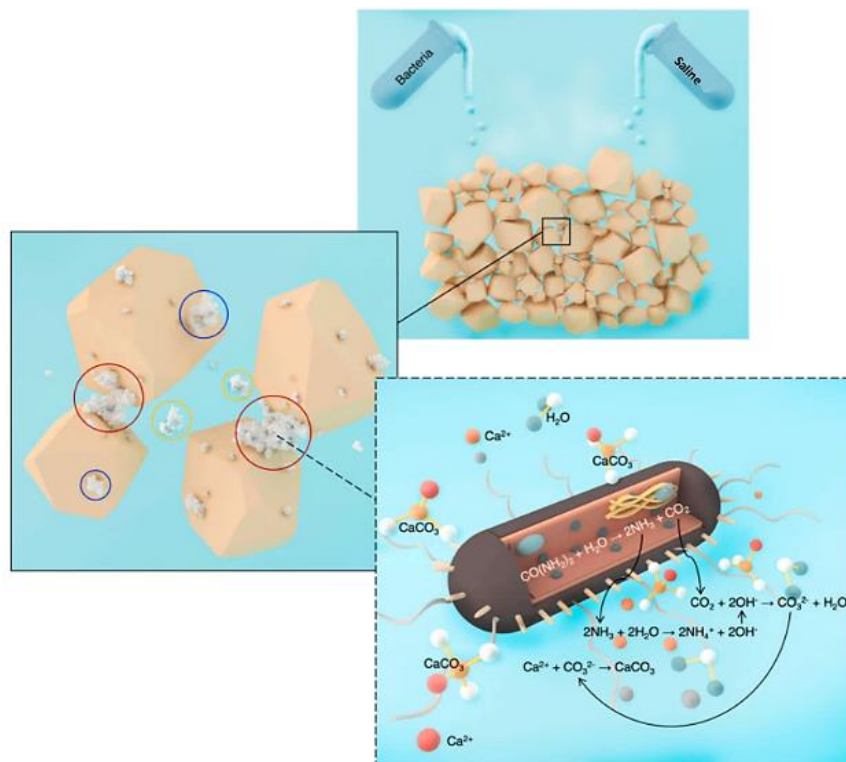


Figure 4. Schematic of MICP-based soil strengthening via ureolysis [12]

2.3. Experimental Setup

The GDS Enterprise Level Dynamic Triaxial Testing System (ELDYN), characterized by its axially rigid load frame and a beam-mounted electromechanical actuator, serves as a sophisticated cyclic apparatus used to assess the cyclic design strength or liquefaction potential of soil samples. The liquefaction test is performed with the aid of specialized apparatus, notably incorporating a triaxial cell testing machine [4, 19]. The test procedure is carried out in the following stages: First, a cylindrical sample measuring 50 × 100 mm is prepared at a representative location where the stabilization material is mixed. The sample is then measured and shaped according to the dimensions to be tested in the laboratory. Next, the sample will be placed in a triaxial cell, which is cylindrical and is recommended to be made of translucent material so that the behavior of the test object can be observed. This cell is designed to facilitate the inflow and outflow of liquid to regulate pressure conditions. Subsequently, the triaxial cell will apply compaction pressure to the sample to simulate pressure conditions. This phase may be designated as the consolidation phase, where the sample is allowed to settle under the compaction pressure. Subsequently, an axial load is applied to the sample to induce shear stresses. The specimen may then undergo cyclic loading, which can be achieved through the use of mechanical or hydraulic actuation within a dynamic system. The degree of cyclic loading applied is contingent upon several factors, including the effective stress that arises following consolidation, the discrepancy between cell and back pressure, the soil type, the soil state, and the loading characteristics, such as frequency and wave type.

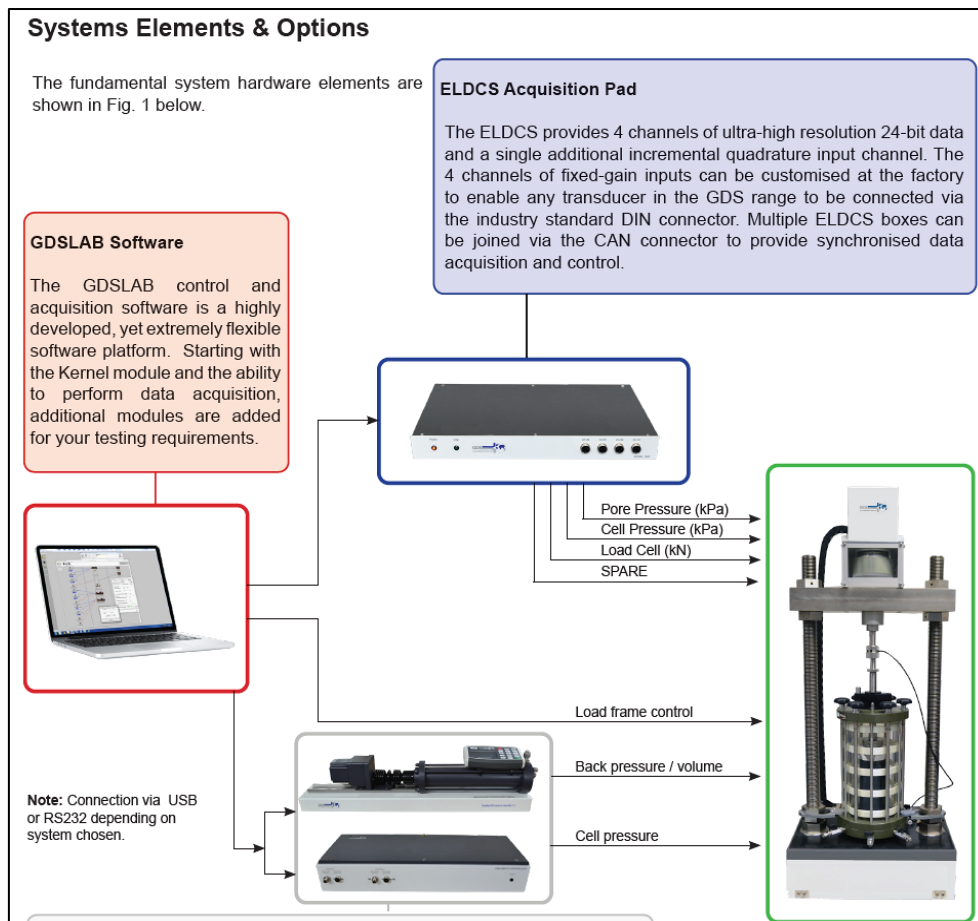


Figure 5. Experimental setup

Thereafter, the triaxial cell will apply compaction pressure to the sample to simulate pressure situations. This phase may be designated as the consolidation phase, where the sample is allowed to settle under the compaction pressure. Subsequently, an axial load is applied to the sample to induce shear stresses. The specimen may then be headed to cyclic loading, which is able to be reached through the use of mechanical or hydraulic actuation within a dynamic system. The degree of cyclic loading applied is contingent upon several factors, including the effective stress that arises following consolidation, the discrepancy between cell and back pressure, the soil type, the soil state, and the loading characteristics, such as frequency and wave type.

3. Methodology

The triaxial cyclic test samples consist of five variations, each representing modeled salinity conditions. These samples have a density of 10% and have been remolded with disturbed soil. Each sample has been mixed with 35% fly ash and 0.2 ml of microbes. The water content in each sample has been situated, and a 23% solution is prepared and left to react for 28 days to allow the cementation procedure to occur. The samples are remolded into five layers of varying compaction, allowing each layer to be compressed to its maximum potential and distributed evenly. The sample preparation procedure is shown in Figure 6.



Figure 6. Sample preparation

As the proportion of saline solution in a given mixture increases, the concentration of sodium chloride (NaCl) also rises, leading to a longer time required for consolidation. This occurs because the mobility of water molecules is reduced as the salinity level in the sample increases. Although minor fluctuations in consolidation time are evident in specimens with varying salinity percentages, it is clear that consolidation proceeds at a slower rate in specimens exhibiting higher salinity levels.

This is due to the lower position of the check valve, which allows a change in volume by the upper to the lower part of the specimen. Figure 7 illustrates the movement of water molecules via red arrows. Moreover, the tests conducted on various samples, which were subjected to salinity situations of 0%, 1%, 2%, and 3.4%, revealed that an increase in salinity percentage corresponded to a significant enhancement in strength. After the consolidation process, a sinusoidal load is applied at a frequency of 1 Hz under undrained conditions, while keeping the cyclic cell pressure and back pressure constant. The cell pressure value is determined based on the optimally saturated sample condition. This frequency, which ranges from 0.1 Hz to 1.5 Hz, is adequate for simulating the impacts of both minor and major earthquakes. The Cyclic Stress Ratio (CSR) can be articulated as follows (see Equation 3):

$$CSR = q_{cyc} / (2\sigma'_c) \tag{3}$$

In this context, q_{cyc} represents cyclic deviatoric stress, whereas σ'_c denotes confining stress.

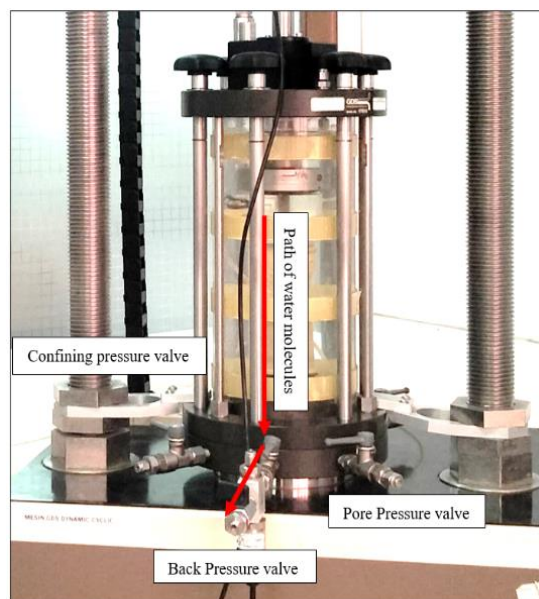


Figure 7. Triaxial cyclic movement of water molecules

By SNI No. 1726 of 2017 regarding earthquake-resistant design procedures for both building and non-building structures at the study site, especially in the Yogyakarta area, the maximum earthquake peak ground acceleration (PGA) value is considered a geometric mean (MCEG) for site class SB, with a PGA value of 0.4-0.5. Based on the research reference above, the cyclic simulation in this study is designed with a vibration frequency of 1 Hz and a cyclic stress ratio (CSR) value of 0.44.

The relative density of the sand used as a benchmark is defined as the relative density reached after the consolidation process (D_r). The relative density after consolidation (D_r) is a critical parameter for design; hence, sand samples were tested to depict three conditions: very loose, loose, and semi-solid. Table 3 illustrates the relationship between relative density and the sand density classification used as a reference in this investigation.

Table 3. Relationship between relative density and sand density classification

N-SPT (number of punches/30 cm)	Relative density, D_r (%)	Density Classification
0 – 4	0 – 20	Very loose
4 – 10	20 – 40	Loose
10 – 30	40 – 60	Medium
30 – 50	60 – 80	Dense
>50	80 – 100	Very dense

4. Results and Discussion

According to the grain distribution graph aligned with Tsuchida's (1970) [29] curve, the results indicate that the soils at the Dominant Point consist of a combination of sand, with grain sizes falling within the liquefaction potential zone. The analysis reveals that as N-SPT values increase, the liquefaction potential decreases. N-SPT values between 4.57 and 26.27 are linked to rising Cyclic Resistance Ratio (CRR) values, which range from 0.05 to 0.4601. With the rise in CRR values, the likelihood of liquefaction diminishes. The research also highlighted a significant potential for liquefaction up to a depth of 15 meters based on SPT data. The correlation among soil parameters suggests that higher N-SPT values result in increased CRR values. Furthermore, a higher earthquake magnitude corresponds to an increased liquefaction potential; for instance, at a magnitude of 6.5 SR, the CRR values exceed those observed at magnitudes of 7.5 SR and 8.5 SR, as shown in Table 4 [28].

The results of this study reveal a positive connection among N-SPT values and the Cyclic Resistance Ratio (CRR), indicating that as N-SPT values increase, CRR values also increase, resulting in a decrease in liquefaction potential. This result aligns by existing theoretical frameworks indicating that denser and more rigid soils, characterized by higher N-SPT values, demonstrate increased resistance to cyclic deformation. The observed CRR range of 0.05 to 0.4601 is consistent with empirical models for granular soils in liquefaction-prone regions. A more nuanced analysis incorporating non-linear regression could provide insights into variations in CRR at varying depths and under different effective confining stresses, particularly within the upper 15 meters where liquefaction potential is most pronounced.

Calculations performed using the determinant method and the soil distribution graph suggest that the study site exhibits a high potential for liquefaction. Therefore, it is crucial to stabilize the soil using a suitable stabilizer. The soil's significant liquefaction potential requires the application of stabilization techniques, specifically biocementing and the MICP method, to enhance its mechanical properties. After this treatment, the soil undergoes a triaxial cyclic test to assess its dynamic resistance. Subsequently, undrained cyclic triaxial (UCT) tests were conducted on specimens consisting of both clean and MICP-treated calcareous sand. Before removing the split mould, the upper and lower surfaces of each specimen were meticulously leveled and positioned on a porous stone, lined with filter paper at the base of the triaxial apparatus pedestal. Afterward, the membrane was delicately rolled over both the top cap and the pedestal, ensuring secure fastening in place with O-rings. Table 5 presents a scenario for assessing liquefaction, considering the impacts of relative density and bridging stress. Within the effective confining stress range of 300 kPa to 700 kPa, the tests included three different salinity variations with a relative density (D_r) of 10-16%, typical of very loose sand.

Table 4. Properties of tested soil and test parameters

Test no.	Variation of salinity (%)	γ_d before (kN/m ³)	e_0	γ_d after (kN/m ³)	B-value	σ'_c (kPa)	CSR	NL
Initial	0	13	0.96	13.05	0.97	700	0.56	43
S0	0	13.4	0.90	13.6	1.0	599.9	0.47	50
S1	1	15.9	0.61	16.2	1	300	0.45	50
S2	2	15.8	0.62	16.4	1	300	0.40	50
S3.4	3.4	13	0.97	13.1	1	600	1.03	20

The process of bio-cementation through microbially induced carbonation precipitation (MICP) modulates the deformation response in specimens treated with MICP by promoting the deposition of calcium carbonate at the points of contact among particles as well as on the surfaces of the sand grains. The deformation response seen in both the untreated sand and the MICP-treated specimens involves compression and dilation strains. Figure 8 shows the axial strain concerning the number of cycles for both specimens. Figure 8 illustrates that, at the beginning of cyclic loading, the axial strain decreases due to the compaction effect resulting by vibration or loading. After this, the specimen transitions into a shear stage characterised by a significant rise in axial strain. Here, the cyclic strength of the specimen becomes the primary factor in the cyclic loading process, especially as the number of cycles approaches the liquefaction threshold. In conclusion, it is evident that during failure, the application of cyclic loading enhances the cyclic strength of the specimen. As liquefaction progresses, a significant increase in axial strain becomes apparent with each cycle. Similar trends were noted across all other tests, thereby supporting previous outcomes [31]. The cyclic testing of the natural soil revealed that the soil showed low resistance to cyclic loading, with failure occurring at the 43rd cycle. The specimens stabilized with fly ash and subjected to varying salinity and MICP treatment showed a decrease in compression strain compared to pure sand while enduring cyclic loading for an extended period. Nevertheless, at a salinity variation of 3.4%, the soil encountered notable failure. The reduced compression strain implies the buildup of hardening due to calcium carbonate precipitation, leading to a decrease in pore space. This outcome is supported by the results of previous research [32].

Table 5. Repeating the determinant method liquefaction potential analysis

Bor hole	Lapisan	H	h	Soil	Gs	amax/g	N- SPT		MSF	Density		rd	σ0	σ0'	CSR	(N1) ₆₀	(N1) _{60 CS}	CRR 6.5	SF	Check		CRR 7.5	SF	Check		CRR 8.5	SF	Check		
		(m)					Blow	cm		vd (kN/m ²)	vsat (kN/m ²)									Determinan Method	Determinan Method			Determinan Method	Determinan Method					
BH 01 A	1	2.5	2.5	Sand	3.36	0.55	10	30	1	15.22	19.72	0.981	49.3	49.3	0.357	11.42	11.42	0.1813	0.507	Liquefaction	0.1259	0.352	Liquefaction	0.0914	0.256	Liquefaction				
	2	9.5	7	Sand	3.09	0.55	23	30	1	15.22	19.72	0.946	138	138	0.345	26.27	26.27	0.4601	1.334	Liquefaction	0.3195	0.926	Liquefaction	0.2319	0.672	Liquefaction				
	3	12	5	Sand		0.55	37	30	1	15.22	19.72	0.962	98.6	98.6	0.35	42.26	42.26	0.2697	0.769	Liquefaction	0.1873	0.534	Liquefaction	0.1359	0.388	Liquefaction				
BH 02 A	1	2.5	2.5	Sand	3.26	0.55	5	30	1	13.63	14.04	0.981	49.3	35.1	0.357	5.71	5.71	0.1115	0.312	Liquefaction	0.0775	0.217	Liquefaction	0.0562	0.157	Liquefaction				
	2	6.5	4	Sand	3.52	0.55	10	30	1	13.63	14.04	0.969	56.16	56.16	0.353	11.42	11.42	0.1813	0.513	Liquefaction	0.1259	0.356	Liquefaction	0.0914	0.259	Liquefaction				
	3	10	6	Sand		0.55	39	30	1	13.63	14.04	0.954	84.24	84.24	0.348	44.55	44.55	0.3318	0.954	Liquefaction	0.2304	0.663	Liquefaction	0.1672	0.481	Liquefaction				
BH 07 A	1	2	2	Sand	3.08	0.55	11	30	1	13.8	14.42	0.985	28.08	28.84	0.359	12.56	12.56	0.1965	0.548	Liquefaction	0.1364	0.380	Liquefaction	0.099	0.276	Liquefaction				
	2	9.5	7.5	Sand	3.13	0.55	21	30	1	13.8	14.42	0.943	108.2	108.2	0.344	23.99	23.99	0.3934	1.145	Liquefaction	0.2732	0.795	Liquefaction	0.1983	0.577	Liquefaction				
	3	13	5.5	Sand		0.55	26	30	1	13.8	14.42	0.958	79.31	79.31	0.349	29.70	29.70	0.645	1.848	Liquefaction	0.4479	1.283	Liquefaction	0.3251	0.931	Liquefaction				
BH 08 A	1	2.5	2.5	Sand	3.29	0.55	7	30	1	13.04	13.04	0.981	36.05	32.6	0.357	8.00	8.00	0.1381	0.386	Liquefaction	0.0959	0.268	Liquefaction	0.0696	0.195	Liquefaction				
	2	8.5	6	Sand	3.34	0.55	16	30	1	13.04	13.04	0.954	78.24	78.24	0.348	18.28	18.28	0.2807	0.807	Liquefaction	0.1949	0.561	Liquefaction	0.1415	0.407	Liquefaction				
	3	15	9	Sand		0.55	22	30	1	13.04	13.04	0.931	117.4	117.4	0.339	25.13	25.13	0.424	1.250	Liquefaction	0.2944	0.868	Liquefaction	0.2137	0.630	Liquefaction				
BH 10 A	1	1.55	1.55	Sandy silt	2.58	0.55	11	30	1	12.43	18.3	0.988	20.21	28.37	0.36	12.56	12.56	0.1965	0.546	Liquefaction	0.1364	0.379	Liquefaction	0.099	0.275	Liquefaction				
	2	3	1.45	Sand	3.04	0.55	15	30	1	12.43	18.3	0.989	26.54	26.54	0.36	17.13	17.13	0.2625	0.728	Liquefaction	0.1823	0.506	Liquefaction	0.1323	0.367	Liquefaction				
	3	6.5	3.5	Sand	2.94	0.55	17	30	1	12.43	18.3	0.973	64.05	64.05	0.355	19.42	19.42	0.2999	0.846	Liquefaction	0.2083	0.587	Liquefaction	0.1512	0.426	Liquefaction				
BH 14 A	1	2.5	2.5	Sand	3.26	0.55	8	30	1	14.06	19.98	0.981	45.75	49.95	0.357	9.14	9.14	0.1521	0.425	Liquefaction	0.1056	0.295	Liquefaction	0.0766	0.214	Liquefaction				
	2	7.5	5	Sand	3.36	0.55	10	30	1	14.06	19.98	0.962	99.9	99.9	0.35	11.42	11.42	0.1813	0.517	Liquefaction	0.1259	0.359	Liquefaction	0.0914	0.261	Liquefaction				
	3	10	5	Sand		0.55	25	30	1	14.06	19.98	0.962	99.9	99.9	0.35	28.56	28.56	0.5626	1.605	Liquefaction	0.3907	1.115	Liquefaction	0.2836	0.809	Liquefaction				
BH 19 A	1	2.5	2.5	Sand	3	0.55	5	30	1	14.47	19.23	0.981	49.95	48.08	0.357	5.71	5.71	0.1115	0.312	Liquefaction	0.0775	0.217	Liquefaction	0.0562	0.157	Liquefaction				
	2	10.5	8	Sand	2.88	0.55	12	30	1	14.47	19.23	0.939	153.8	153.8	0.342	13.71	13.71	0.2121	0.620	Liquefaction	0.1473	0.431	Liquefaction	0.1069	0.313	Liquefaction				
	3	12.5	2	Sand	3.01	0.55	15	30	1	14.47	19.23	0.985	38.46	38.46	0.359	17.13	17.13	0.2625	0.731	Liquefaction	0.1823	0.508	Liquefaction	0.1323	0.369	Liquefaction				
	4	16.5	4	Sand	3.91	0.55	23	30	1	14.47	19.23	0.969	76.92	76.92	0.353	26.27	26.27	0.4601	1.302	Liquefaction	0.3195	0.904	Liquefaction	0.2319	0.657	Liquefaction				
BH 20 A	1	3.5	3.5	Sand	3.42	0.55	4	30	1	15.51	19.5	0.973	67.31	68.25	0.355	4.57	4.57	0.0992	0.280	Liquefaction	0.0689	0.194	Liquefaction	0.05	0.141	Liquefaction				
	2	8.5	5	Sand	2.83	0.55	9	30	1	15.51	19.5	0.962	97.5	97.5	0.35	10.28	10.28	0.1665	0.475	Liquefaction	0.1156	0.330	Liquefaction	0.0839	0.239	Liquefaction				
	3	16	11	Sand		0.55	27	30	1	15.51	19.5	0.916	214.5	214.5	0.334	30.84	30.84	0.7781	2.331	Liquefaction	0.5404	1.619	Liquefaction	0.3922	1.175	Liquefaction				

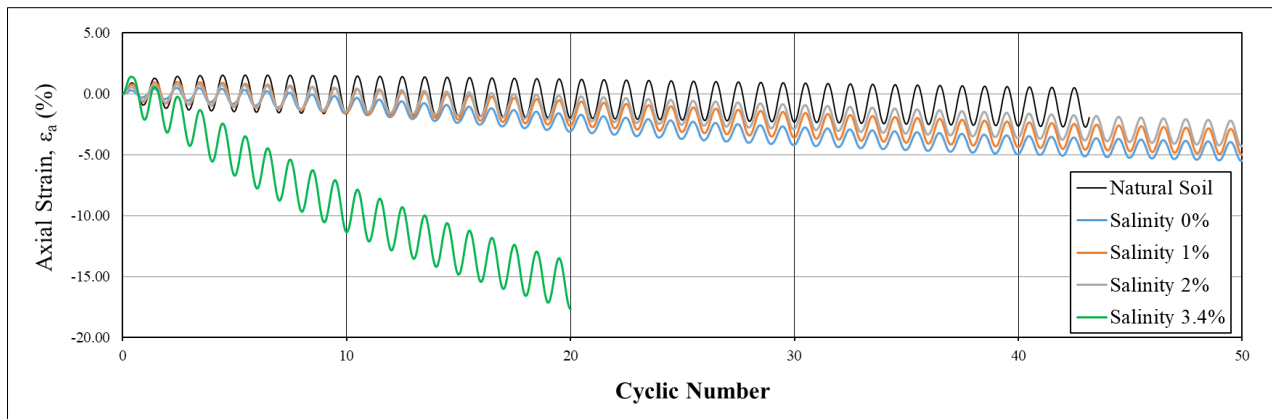


Figure 8. Strain development in salinity-treated soil and MICP-treated specimens

Figure 9 shows the relationship between the number of cycles and the r_u values for both untreated and MICP-treated specimens. The assessment and analysis of pore pressure accumulation within the treated specimen offer valuable insights into the mechanical response observed during the MICP treatment process. When the specimen nears liquefaction, a distinct notch becomes visible, indicating the cyclic behavior of the specimen under cyclic loading conditions. The region encompassed by the aforementioned notch between the two peaks acts as a measure of the specimen's cyclic activity. It is important to note that as axial strain increases, the notch area also enlarges, indicating an increase in cyclic activity linked to a higher number of cycles. This observation is consistent with the findings of previous research [33, 34]. A noteworthy pattern emerges in the gradual buildup of pore pressure preceding the liquefaction stage, which is then followed by an abrupt surge in pore pressure after liquefaction occurs. The number of cycles needed for liquefaction rises with an increase in calcium carbonate precipitation. Calcium carbonate deposition inside the treated specimen effectively interlocks pore spaces, impeding the dissipation of pore pressure and consequently leading to a higher number of cycles required for liquefaction to occur. When described by the r_u ratio in terms of liquefaction behavior, the r_u value reaches 0.80. whereas, in limited liquefaction behavior, the r_u value is only 0.70–0.90. Figure 9 illustrates the behavior of loose sandy soils by relative density (D_r) values of 13–16% under situations of very loose consistency, by varying respective confining stresses. The integration of microbial-induced calcium carbonate precipitation (MICP) has shown a significant improvement in soil stability, primarily by depositing calcium carbonate at particle contact points. The decrease in compression strain and the higher cyclic resistance seen in the MICP-treated specimens indicate enhanced soil rigidity and interparticle bonding. Notably, at 1% salinity, the stabilized soil showed a marked improvement in resistance to liquefaction, requiring up to 14 cycles for liquefaction initiation at an r_{ur_uru} value of 0.8. However, the outcomes suggest that salinity levels beyond 3.4% diminish the efficiency of MICP, potentially due to osmotic stress on microbial activity, as suggested in studies by Liu et al. [35]. Further investigation into the biochemical mechanisms influenced by different salinity levels could enhance the optimization of the MICP procedure for various soil conditions.

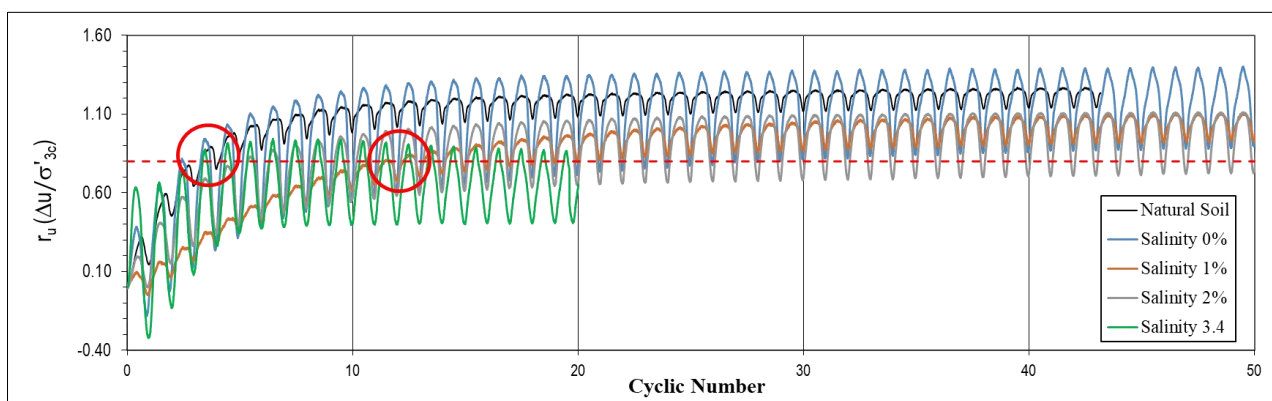


Figure 9. Pore pressure development in soil treated with salinity and MICP-treated specimen

Figure 10 depicts the hysteresis loop of deviatoric stress versus axial strain for both clean sand and MICP-treated specimens. Upon unloading or reversing cyclic loading, the elastic deformation is restored; yet, the remaining work is carried out by the rearrangement of the soil structure, leading to the accumulation of axial strain. Because loading and unloading follow distinct paths in cyclic loading, a hysteresis loop is created. The area enclosed by this loop offers a gauge of the energy dissipated in a single loading cycle for both the pure sand and the MICP-treated sand specimens. Notably, the MICP-treated specimen exhibits a larger hysteresis loop, which is attributed to the bio-cementation effect. This effect becomes more pronounced with increasing cycles.

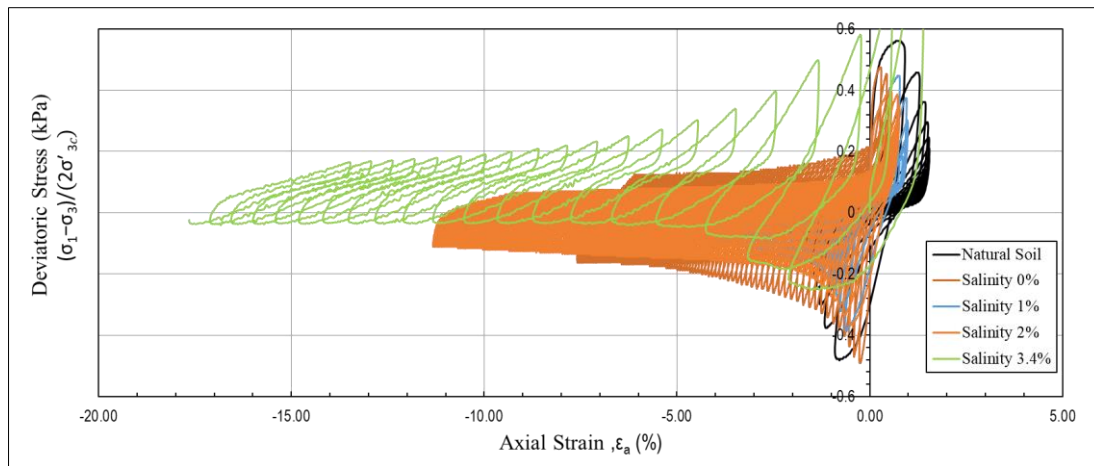


Figure 10. Stress-Strain development at Salinity treatment soil and MICP-treated specimen

Figure 11 depicts the deviatoric stress and the effective stress path for both untreated and MICP-treated specimens composed of pure sand. A discernible trend emerges as the effective stress path progresses from right to left, primarily influenced by the decline in the mean effective stress concomitant with the increase in pore water pressure under cyclic loading. Once the mean effective stress reaches a non-zero state and intersects with the effective failure envelope, liquefaction is initiated. At this point, the specimen's structural rigidity is completely diminished, making it unable to withstand any additional deviatoric stress. Comparatively, the MICP-treated specimen showed a significantly higher number of cycles required for liquefaction than the untreated sand specimen. This indicates that the MICP-treated specimen has improved cyclic shear resistance due to calcium carbonate precipitation at the contact points among particles and the formation of calcite particles. The cyclic loading tests revealed significant differences in the hysteresis loop between untreated and MICP-treated specimens. The larger hysteresis loop in the treated specimens reflects increased elastic deformation and energy storage capacity, corroborating the bio-cementation effect observed in prior studies [36-38]. This behavior suggests that MICP-treated soils dissipate less energy during cyclic deformation due to enhanced interparticle bonding. Quantifying the energy dissipation per cycle and correlating it by calcium carbonate precipitation levels could provide a deeper understanding of the mechanical benefits conferred by MICP treatment.

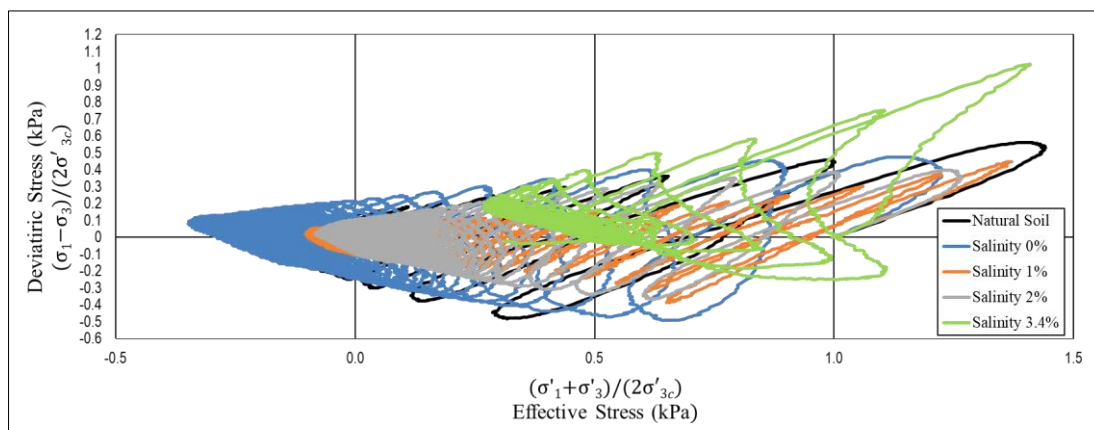


Figure 11. Cyclic Deformation characteristics of Salinity-treated soil and MICP-treated specimen

The efficacy of MICP treatment in cyclic resistance can be evaluated by conducting a microstructural analysis. In the case of pure sand, no calcium carbonate deposition is observed on the surface, leading to the lack of interlocking among soil particles and a significant pore space among sand grains after curing for 28 days. The MICP treatment has been observed to enhance the bonding effect of particle-to-particle contact, as well as particle-to-calcite (surface deposition). This can be seen in the SEM images (Figure 12). Following that, the corresponding SEM images were headed to XRD analysis to estimate the concentration of minerals like silica and calcium. The XRD analysis of pure sand revealed that silica was the predominant mineral present, with no detectable traces of calcium minerals. In contrast, samples treated with MICP displayed the presence of minerals such as silica, calcium, and chloride (Figure 13). This analysis demonstrates how the increase in roughness and interlocking of the sand grains, resulting from the precipitation of calcium carbonate, is reflected in the XRD results, which can be seen in Table 6. As the precipitation of calcium carbonate intensifies, the interlocking of soil grains becomes more pronounced, potentially resulting in a transition toward a more rock-like structure (Amorphous 86.05%; Degree of Crystallinity 13.95%).

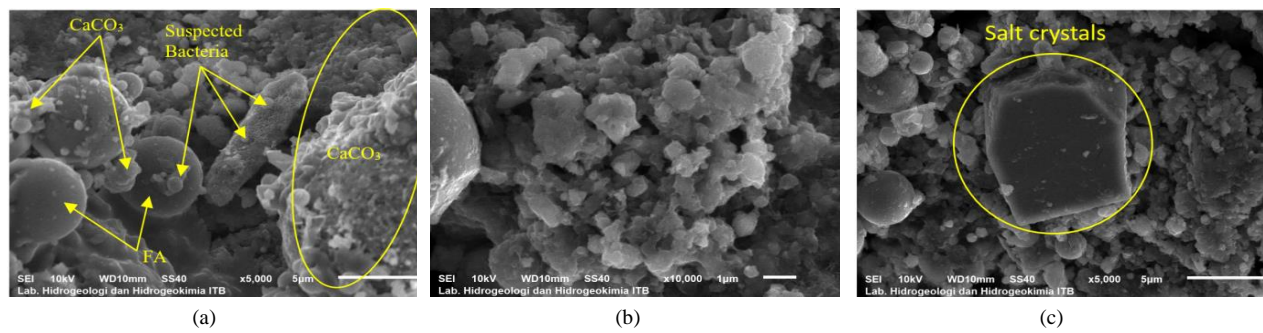


Figure 12. SEM scanning for stabilized soil, (a) 5000x zoom, (b) 10000x zoom, (c) 5000x zoom

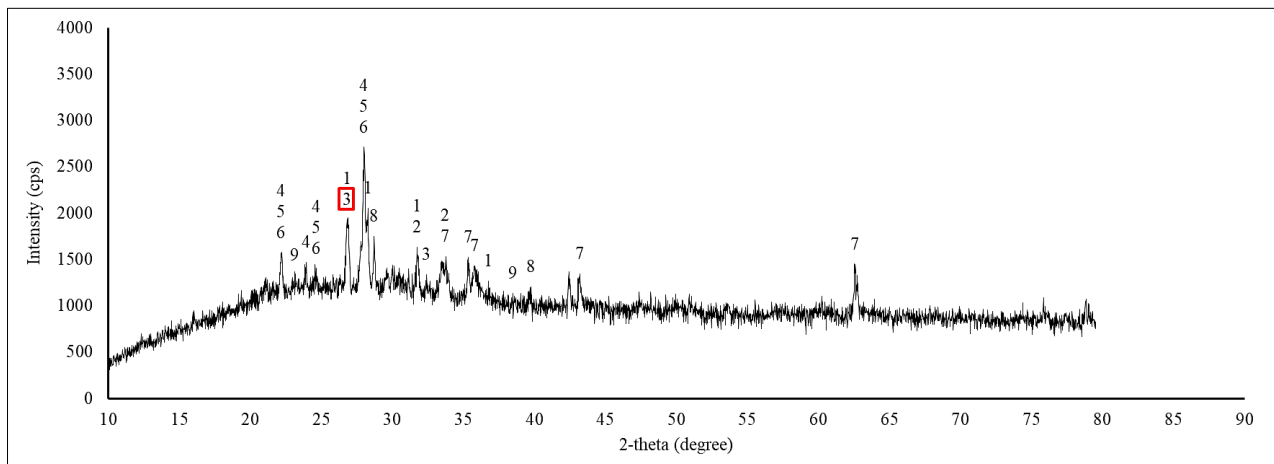


Figure 13. XRD test result for stabilized soil

Table 6. Chemical composition of XRD results

Code	Minerals name	Chemical composition	Percentage	Total	Total by DOC	
1	CSH	Afwilite	Ca ₃ Si ₂ O ₁₀ H ₆	5.5%	15.7%	2.19%
		Ca ₂ SiO ₃ H ₂	Ca ₂ SiO ₃ H ₂	10.2%		
2	CASH	Zoisite	Ca ₂ Al ₃ Si ₃ O ₁₃ H	22.3%	22.3%	3.11%
3	CaCO ₃	Vaterite	CaCO ₃	10.3%	10.3%	1.44%
4	Quartz	Quartz	SiO ₂	11.5%	11.5%	1.60%
5	Albite	Albite	NaAlSi ₃ O ₈	15.2%	15.2%	2.12%
6	Anorthite	Anorthite	CaAl ₂ Si ₂ O ₈	16.7%	16.7%	2.33%
		Hematite	Fe ₂ O ₃	2.1%	8.3%	1.16%
7	Iron	Magnesiowuestite	Fe _{0.4} Mg _{0.6} O	3.6%		
		Magnetite	Fe ₃ O ₄	2.6%		
8	Halite	Halite-sylvite	Cl K _{0.8} N _{0.2}			
9	Sodium Chlorate	Sodium Chlorate	NaClO ₃			
				100%	13.95%	

In addition to these extensive studies, it is imperative to conduct further investigations at the molecular level to achieve a more comprehensive understanding of the fundamental chemical procedures and biological mechanisms involved. This understanding is fundamental to optimizing calcium carbonate (CaCO₃) redispersion in soils using this specific method. By exploring these intricate mechanisms, researchers can carry out more precise experiments customized to different scenarios and specific needs. Among the techniques commonly employed in studies of microbial-induced calcium carbonate precipitation (MICP), X-ray diffraction (XRD) is particularly valuable as an analytical tool. This approach offers insights into the crystalline structure and composition of CaCO₃, allowing researchers to gain a deeper understanding of the redispersion process and enhance it. The SEM and XRD analyses provided crucial evidence of the microstructural transformation induced by MICP treatment. The precipitation of calcium carbonate increased surface roughness and interlocking among soil particles, resulting in a transition towards a rock-like structure. The XRD analysis revealed a significant presence of minerals such as vaterite, albite, and anorthite, which contribute to the improved mechanical properties. These results are in line with the research conducted by Wang

et al. [22], emphasizing the importance of calcium carbonate in enhancing soil strength. Future research should concentrate on quantifying the degree of crystallinity and its correlation with cyclic resistance to better understand the mechanisms supporting MICP effectiveness.

This study expands on and enhances the findings of Tsuchida (1970) [29] by offering a comprehensive analysis of soil behavior under different levels of seismic activity. In contrast to prior studies that mainly concentrated on empirical liquefaction thresholds, this research incorporates advanced stabilization methods and assesses their effectiveness under practical loading conditions. The observed increase in cyclic resistance due to MICP treatment complements outcomes by Liu et al. [35], who demonstrated the impact of soil structure rearrangement on deformation characteristics. Additionally, the influence of salinity on the effectiveness of bio-cementation introduces a novel dimension, filling a critical gap in the literature.

The high liquefaction potential observed at the study site emphasizes the need for soil stabilization to mitigate seismic risks. The findings support the use of MICP as a sustainable and effective stabilization method, especially in coastal or saline settings. Subsequent research should examine the molecular dynamics of microbial activity in diverse environmental conditions, along with the long-term resilience of bio-cemented soils under cyclic and static loading scenarios. Advanced modeling techniques, like discrete element modeling (DEM), could further clarify the micro-mechanical processes that govern the observed macroscopic behavior.

5. Conclusion

This study showcases the efficacy of Microbial-Induced Calcium Precipitation (MICP) as a sustainable method to improve the dynamic resistance of soils prone to liquefaction, especially in diverse salinity conditions. By integrating *Bacillus Safensis*. microbes and fly ash into the biocementation procedure, the research highlights significant improvements in soil stability and cyclic resistance, as evidenced by triaxial cyclic testing. The results indicate that untreated soils in seismic zones, like Yogyakarta International Airport, are highly prone to liquefaction, by failure occurring inside of a few cycles. In contrast, MICP-treated soils display increased stiffness, reduced compressive strain, and enhanced cyclic resistance, particularly at 1% salinity, where liquefaction was delayed up to 14 cycles.

The research emphasizes the crucial impact of salinity in optimizing the MICP process. While low salinity levels facilitate enhanced biocementation and soil resistance, higher salinity levels (e.g., 3.4%) hinder microbial activity due to osmotic stress, reducing the efficiency of calcium carbonate deposition. Scanning Electron Microscopy (SEM) and X-Ray Diffraction (XRD) analyses support the enhancements in microstructure, demonstrating particle interlocking and reduction in pore space from calcite precipitation. These microstructural changes aid in shifting soil properties towards rock-like behavior under dynamic loads. This research fills a crucial gap in comprehending the interaction between salinity and MICP effectiveness in cyclic loading scenarios typical of seismic activity. Future studies should delve into the biochemical mechanisms of microbial activity in diverse environmental conditions, as well as the long-term performance and scalability of MICP-treated soils in different geological settings.

6. Declarations

6.1. Author Contributions

Conceptualization, N.A.D. and R.A.S.; methodology, N.A.D. and R.A.S.; validation, N.A.D., R.A.S., J.E.P., T.R.S., and D.D.W.; formal analysis, N.A.D.; investigation, N.A.D.; resources, N.A.D.; data curation, N.A.D.; writing—original draft preparation, N.A.D.; writing—review and editing, N.A.D.; visualization, N.A.D.; supervision, N.A.D.; project administration, N.A.D.; funding acquisition, B.P.P.T. and L.P.D.P. All authors have read and agreed to the published version of the manuscript.

6.2. Data Availability Statement

The data presented in this study are available in the article.

6.3. Funding and Acknowledgements

The researchers wish to express their sincere gratitude to Indonesian Education Scholarship (BPI), Center for Higher Education Funding and Assessment (PPAPT) and the Indonesia Endowment Fund for Education (LPDP) for their invaluable financial support. Furthermore, they extend their heartfelt gratitude to the experts whose insightful recommendations were instrumental in enhancing both the content and overall quality of this study. Furthermore, the authors wish to acknowledge the support provided by Janabadra University, particularly in terms of funding, as well as the Department of Civil Engineering at Sepuluh Nopember Institute of Technology and PT. Soilens Indonesia for their assistance in facilitating the laboratory testing conducted in this study. Risa, D.A., for her contributions in editing the English language. Additionally, Gratitude is extended to Mr. Makno Basoeki provides safensis nutrition and Prof. Davin H. E. Setiamarga isolates bacteria.

6.4. Conflicts of Interest

The authors declare no conflict of interest.

7. References

- [1] Amipour, S., Khashila, M., Bayoumi, A., Karray, M., & Chekired, M. (2022). Specimens size effect D/H on cyclic behaviour and liquefaction potential of clean sand. *Acta Geotechnica*, 17(5), 2047–2057. doi:10.1007/s11440-021-01339-x.
- [2] Farooq, M. A., & Nimbalkar, S. (2024). Monotonic and cyclic triaxial testing of untreated and polyurethane-treated soil and soil-rubber mixtures. *Acta Geotechnica*, 19(2), 605–630. doi:10.1007/s11440-023-02100-2.
- [3] Khashila, M., Hussien, M. N., Chekired, M., & Karray, M. (2021). On the Dynamic Soil Behavior under Triaxial and Simple Shear Modes. *International Journal of Geomechanics*, 21(8), 04021134. doi:10.1061/(asce)gm.1943-5622.0002085.
- [4] Wang, W., He, X., Wu, S., & Chu, J. (2024). Presence of Mg-calcite and its influence on MICP and EICP processes. *Journal of Rock Mechanics and Geotechnical Engineering*, 1-12. doi:10.1016/j.jrmge.2024.09.045.
- [5] Smitha, S., & Rangaswamy, K. (2020). Effect of Biopolymer Treatment on Pore Pressure Response and Dynamic Properties of Silty Sand. *Journal of Materials in Civil Engineering*, 32(8), 04020217. doi:10.1061/(asce)mt.1943-5533.0003285.
- [6] Smitha, S., Rangaswamy, K., & Keerthi, D. S. (2021). Triaxial test behaviour of silty sands treated with agar biopolymer. *International Journal of Geotechnical Engineering*, 15(4), 484–495. doi:10.1080/19386362.2019.1679441.
- [7] Kassas, K., Adamidis, O., & Anastasopoulos, I. (2021). Shallow strip foundations subjected to earthquake-induced soil liquefaction: Validation, modelling uncertainties, and boundary effects. *Soil Dynamics and Earthquake Engineering*, 147, 106719. doi:10.1016/j.soildyn.2021.106719.
- [8] Zhu, L., Yang, Q., Luo, L., & Cui, S. (2022). Pore-Water Pressure Model for Carbonate Fault Materials Based on Cyclic Triaxial Tests. *Frontiers in Earth Science*, 10, 1–12. doi:10.3389/feart.2022.842765.
- [9] Zhu, M., Kong, F., Li, Y., Li, M., Zhang, J., & Xi, M. (2020). Effects of moisture and salinity on soil dissolved organic matter and ecological risk of coastal wetland. *Environmental Research*, 187, 109659. doi:10.1016/j.envres.2020.109659.
- [10] Rifa'i, A., Fathani, T. F., & Adi, A. D. (2024). Post-Earthquake Liquefaction Vulnerability Mapping by Swedish Weight Sounding and Standard Penetration Test. *Civil Engineering Journal*, 10(7), 2216-2232. doi:10.28991/CEJ-2024-010-07-09.
- [11] Xu, K., Huang, M., Liu, Z., Cui, M., & Li, S. (2023). Mechanical properties and disintegration behavior of EICP-reinforced sea sand subjected to drying-wetting cycles. *Biogeotechnics*, 1(2), 100019. doi:10.1016/j.bgtech.2023.100019.
- [12] Fu, T., Saracho, A. C., & Haigh, S. K. (2023). Microbially induced carbonate precipitation (MICP) for soil strengthening: A comprehensive review. *Biogeotechnics*, 1(1), 100002. doi:10.1016/j.bgtech.2023.100002.
- [13] Yu, X., Tan, Y., Song, W., Kemeny, J., Qi, S., Zheng, B., & Guo, S. (2024). Damage evolution of rock-encased-backfill structure under stepwise cyclic triaxial loading. *Journal of Rock Mechanics and Geotechnical Engineering*, 16(2), 597–615. doi:10.1016/j.jrmge.2023.11.015.
- [14] Voyagaki, E., Kishida, T., Aldulaimi, R. F., & Mylonakis, G. (2023). Integration and calibration of UBCSAND model for drained monotonic and cyclic triaxial compression of aggregates. *Soil Dynamics and Earthquake Engineering*, 171, 107978. doi:10.1016/j.soildyn.2023.107978.
- [15] Wang, P., Zhang, N., Wei, Q., Xu, X., Cui, G., Li, A., Yang, S., & Kan, J. (2024). Mechanical responses of anchoring structure under triaxial cyclic loading. *Journal of Rock Mechanics and Geotechnical Engineering*, 16(2), 545–560. doi:10.1016/j.jrmge.2023.04.020.
- [16] Molina-Gómez, F., Viana da Fonseca, A., Ferreira, C., & Caicedo, B. (2023). Improvement of cyclic liquefaction resistance induced by partial saturation: An interpretation using wave-based approaches. *Soil Dynamics and Earthquake Engineering*, 167, 107819. doi:10.1016/j.soildyn.2023.107819.
- [17] Jain, A., Mittal, S., & Shukla, S. K. (2023). Liquefaction proneness of stratified sand-silt layers based on cyclic triaxial tests. *Journal of Rock Mechanics and Geotechnical Engineering*, 15(7), 1826-1845. doi:10.1016/j.jrmge.2022.09.015.
- [18] Diana, N. A., Soemitro, R. A. A., Ekaputri, J. J., Satrya, T. R., & Warnana, D. D. (2024). The influence of variations in salinity levels on the biocementing process on soil improvement of liquefaction potential. *IOP Conference Series: Earth and Environmental Science*, 1372(1), 012071. doi:10.1088/1755-1315/1372/1/012071.
- [19] Song, Z., Wu, C., Li, Z., & Shen, D. (2024). Fracture sealing based on microbially induced carbonate precipitation and its engineering applications: A review. *Biogeotechnics*, 2(4), 100100. doi:10.1016/j.bgtech.2024.100100.
- [20] Weng, Y., Lai, H., Zheng, J., Cui, M., Chen, Y., Xu, Z., Jiang, W., Zhang, J., & Song, Y. (2024). Effect of acid type on biomineralization of soil using crude soybean urease solution. *Journal of Rock Mechanics and Geotechnical Engineering*, 5135-5146. doi:10.1016/j.jrmge.2024.09.017.

- [21] Kuo, C. H., Huang, J. Y., Lin, C. M., Chen, C. Te, & Wen, K. L. (2021). Near-surface frequency-dependent nonlinear damping ratio observation of ground motions using SMART1. *Soil Dynamics and Earthquake Engineering*, 147, 106798. doi:10.1016/j.soildyn.2021.106798.
- [22] Wang, Y., Soga, K., DeJong, J. T., & Kabla, A. J. (2021). Effects of Bacterial Density on Growth Rate and Characteristics of Microbial-Induced CaCO₃ Precipitates: Particle-Scale Experimental Study. *Journal of Geotechnical and Geoenvironmental Engineering*, 147(6), 04021036. doi:10.1061/(asce)gt.1943-5606.0002509.
- [23] Mijic, Z., Bray, J. D., Riemer, M. F., Rees, S. D., & Cubrinovski, M. (2021). Cyclic and monotonic simple shear testing of native Christchurch silty soil. *Soil Dynamics and Earthquake Engineering*, 148, 106834. doi:10.1016/j.soildyn.2021.106834.
- [24] Quintero, J., Gomes, R. C., Rios, S., Ferreira, C., & Viana da Fonseca, A. (2023). Liquefaction assessment based on numerical simulations and simplified methods: A deep soil deposit case study in the Greater Lisbon. *Soil Dynamics and Earthquake Engineering*, 169. doi:10.1016/j.soildyn.2023.107866.
- [25] Peellage, W. H., Fatahi, B., & Rasekh, H. (2023). Assessment of cyclic deformation and critical stress amplitude of jointed rocks via cyclic triaxial testing. *Journal of Rock Mechanics and Geotechnical Engineering*, 15(6), 1370–1390. doi:10.1016/j.jrmge.2023.02.001.
- [26] Dejong, J. T., Soga, K., Kavazanjian, E., Burns, S., Van Paassen, L. A., AL Qabany, A., Aydilek, A., Bang, S. S., Burbank, M., Caslake, L. F., Chen, C. Y., Cheng, X., Chu, J., Ciurli, S., Esnault-Filet, A., Fauriel, S., Hamdan, N., Hata, T., Inagaki, Y., ... Weaver, T. (2013). Biogeochemical processes and geotechnical applications: Progress, opportunities and challenges. *Geotechnique*, 63(4), 287–301. doi:10.1680/geot.SIP13.P.017.
- [27] Yang, C., Lv, D., Jiang, S., Lin, H., Sun, J., Li, K., & Sun, J. (2021). Soil salinity regulation of soil microbial carbon metabolic function in the Yellow River Delta, China. *Science of the Total Environment*, 790, 148258. doi:10.1016/j.scitotenv.2021.148258.
- [28] Diana, N. A., Soemitro, R. A. A., Ekaputri, J. J., Satrya, T. R., & Warnana, D. D. (2024). Evaluation of Liquefaction Risk Based on Soil Grain Size Characteristics and Standard Penetration Test (N-SPT) Resistance Results Case Study of Yogyakarta International Airport. *Publication of Civil Engineering Orientation Research (Protection)*, 6(1), 51–58. doi:10.26740/proteksi.v6n1.p51-58. (In Indonesian).
- [29] Tsuchida, H. (1970). Prediction and countermeasure against the liquefaction in sand deposits. Abstract of the seminar in the Port and Harbor Research Institute, Kanagawa, Japan.
- [30] Miyamoto, M., Tsuchida, H., Sakuraya, N., Omote, T., Iwasaki, H., & Namiki, A. (1988). Changes of liver function following prolonged general anesthesia. *The Journal of Japan Society for Clinical Anesthesia*, 8(3), 284-288.
- [31] Gitanjali Kennedy, A., Ge, L., & Jhuo, Y.-S. (2024). Experimental Study of Ground Improvement Using Enzyme Induced Calcite Precipitation (EICP). *Japanese Geotechnical Society Special Publication*, 10(51), 1918–1923. doi:10.3208/jgssp.v10.os-40-04.
- [32] Xiao, Y., He, X., Zaman, M., Ma, G., & Zhao, C. (2022). Review of Strength Improvements of Biocemented Soils. *International Journal of Geomechanics*, 22(11), 1–23. doi:10.1061/(asce)gm.1943-5622.0002565.
- [33] Yao, C. R., Wang, B., Liu, Z. Q., Fan, H., Sun, F. H., & Chang, X. H. (2019). Evaluation of liquefaction potential in saturated sand under different drainage boundary conditions-An energy approach. *Journal of Marine Science and Engineering*, 7(11), 411. doi:10.3390/jmse7110411.
- [34] Zhang, J., Bilotta, E., Sun, Q., & Yuan, Y. (2024). Numerical simulation and parametric analysis on a shallow tunnel in liquefiable ground subject to multiple shakings. *Soil Dynamics and Earthquake Engineering*, 183, 108802. doi:10.1016/j.soildyn.2024.108802.
- [35] Liu, C., Yuan, Y., He, W., & Zhang, L. (2019). Durability analysis of seashore saline soil bound with a slag compound binder. *Soils and Foundations*, 59(5), 1456–1467. doi:10.1016/j.sandf.2019.06.005.
- [36] Mustafa, H., Maulana, A., Irfan, U. R., & Tonggiroh, A. (2023). The geoelectric approach to analyzing the profile of post-mining nickel laterite deposits in the Motui District, North Konawe Regency, Indonesia. *IOP Conference Series: Earth and Environmental Science*, 1134(1), 012035. doi:10.1088/1755-1315/1134/1/012035.
- [37] Rahman, M. M., Hora, R. N., Ahenkorah, I., Beecham, S., Karim, M. R., & Iqbal, A. (2020). State-of-the-art review of microbial-induced calcite precipitation and its sustainability in engineering applications. *Sustainability (Switzerland)*, 12(15), 6281. doi:10.3390/SU12156281.
- [38] Lai, H., Ding, X., Cui, M., Zheng, J., Chu, J., Chen, Z., & Zhang, J. (2024). A new bacterial concentration method for large-scale applications of biomineralization. *Journal of Rock Mechanics and Geotechnical Engineering*, 16(12), 5109-5120. doi:10.1016/j.jrmge.2024.01.015.